Proceedings of Meetings on Acoustics

Volume 12, 2011 http://acousticalsociety.org/

161st Meeting
Acoustical Society of America
Seattle, Washington
23 - 27 May 2011
Session 5pPA: Physical Acoustics

5pPA10. Experimental investigation of a characteristic shock formation distance in finite-amplitude noise propagation

Michael Muhlestein* and Kent Gee

***Corresponding author's address: Physics and Astronomy, Brigham Young University, N283 ESC, Provo, UT 84602, mimuhle@gmail.com**

Unlike initially sinusoidal waveforms, the definition of the "shock formation distance" for noise is complicated by the fact that not all shocks form at the same rate. Examination of the concept of a "characteristic" shock formation distance for noise raises some questions: Is there some generalization of the shock formation distance for sinusoidal signals that can be applied to noise? If so, is it inversely proportional to amplitude and frequency, as the pure tone distance is? In this study, initially sinusoidal, narrowband, and broadband noise data have been acquired using 3.18 mm microphones flush mounted along the walls of an anechoically terminated plane-wave tube. The behavior of the time derivative statistics for the sine-wave tests has been used to guide formulation of a statistical definition of a characteristic shock formation distance for initially Gaussian noise.

Published by the Acoustical Society of America through the American Institute of Physics

Received 6 Jun 2011; published 22 Jun 2011
Proceedings of Meetings on Acoustics, Vol. 12, 045002 (2011)

I. INTRODUCTION

There are important sources of finite-amplitude broadband noise, such as the jets from military aircraft[1,2] or rockets.[3,4,5] One important characterization of finite-amplitude sound fields is the onset of shocks. Due to nonlinear waveform steepening, acoustic shocks will form as the wave propagates. Previous work has introduced several useful characteristic nonlinear distortion lengths. Most common is the shock formation distance[6] for an initially sinusoidal signal, which is defined as

$$\bar{x}_S = \frac{\rho_0 c_0^3}{\beta \omega p_0} \tag{1}$$

where p_0 is the amplitude of the sine wave, ρ_0 is the ambient air density, c_0 is the small signal speed of sound, β is the coefficient of nonlinearity, and ω is the sine-wave frequency in rad/s. Following the same form, Gurbatov and Rudenko[7] defined a "characteristic distortion distance" for narrowband noise, replacing p_0 with σ_p, the standard deviation of the pressure, and ω with ω_0, the central frequency. This length will be called $\bar{x}_N$ in this paper. Note that σ_p is equal to the rms pressure. They further defined a "nonlinear distortion length" for broadband noise using a characteristic frequency, ω_c. This length will be called $\bar{x}_B$ in this paper. These distances are summarized in Table 1.

	Sinusoidal Signal	Narrowband Noise	Broadband Noise
$p\|_{x=0}$	$p_0 \sin(\omega t + \phi)$	$\Delta\omega \ll \omega_0$	$\Delta\omega \sim \omega_c$
$\bar{x}$	$\bar{x}_S = \frac{\rho_0 c_0^3}{\beta \omega p_0}$	$\bar{x}_N = \frac{\rho_0 c_0^3}{\beta \omega_0 \sigma_p}$	$\bar{x}_B = \frac{\rho_0 c_0^3}{\beta \omega_c \sigma_p}$
$\lim_{\Delta\omega \to 0} \bar{x}$	$\frac{\bar{x}_N}{\sqrt{2}}$	$\bar{x}_N$	$\bar{x}_N$

Table 1. Summary of "nonlinear distortion lengths" for various signals. Notice that the definitions for $\bar{x}$ for narrowband noise and broadband noise both depend on the standard deviation of the pressure (rms pressure) rather than the peak pressure as in the sinusoidal case. This causes $\bar{x}_N$ and $\bar{x}_B$ to be consistently larger than $\bar{x}_S$ for a given overall sound pressure level and central or characteristic frequency.

Some observations at the outset are worthwhile. First of all, one may note that the definitions for $\bar{x}_N$ and $\bar{x}_B$ do not reduce to $\bar{x}_S$ as the noise bandwidth goes to zero. This is illustrated in the bottom row of Table 1. This does not immediately disqualify consistency, however, because the amplitude distribution of the noise must necessarily change from Gaussian to bimodal[8,9] as $\Delta\omega \to 0$ and the sinusoidal case is recovered. Secondly, Pernet and Payne[10] found that harmonic generation was accelerated for narrowband noise relative to pure tones. This implies that shocks, which have very high frequency content, would develop closer to the source. However the definition for $\bar{x}_N$ suggests that shocks in narrowband noise of the same overall level will shock farther from the source than would a sine wave. Thirdly, nonlinearity emphasizes pressure outliers,[7] which is ignored by the use of the rms pressure.

It is important to note that $\bar{x}_N$ and $\bar{x}_B$ were defined for convenience to be as similar as possible to the sinusoidal shock formation distance in Eq. (1); they were not purported by their authors to be equivalent to a shock formation distance. However, because of their designed similarities to Eq. (1) and their being denoted as "nonlinear distortion lengths," the question should be asked, are these distances consistent with a "characteristic" shock formation distance? Or, is there a definition of a characteristic shock formation distance which can be more appropriately termed a "nonlinear distortion length" for initially Gaussian noise (which are traditionally the same thing for the initially sinusoidal case) And if there is a "characteristic" shock formation distance, would it be inversely proportional to amplitude and frequency, as the sinusoidal case is? We would like to answer these questions.

II. EXPERIMENT

In order to examine $\bar{x}_N$ and $\bar{x}_B$ relative to $\bar{x}_S$, a plane-wave tube was constructed (see Fig. 1). We used 5.08 cm diameter PVC pipe in 3.05 m coupled increments to build a tube that is 19.8 m long. Microphones (3.18 mm (1/8 inch) G.R.A.S. pressure microphones with the grid caps removed) were inserted to be flush with the inside wall at various distances. The first microphone was about 10 cm from the source (a BMS 4592 compression driver), and the farthest microphone was 11.8 m from the source. The tube has an anechoic termination made of fiberglass that is 1.26 m in length.

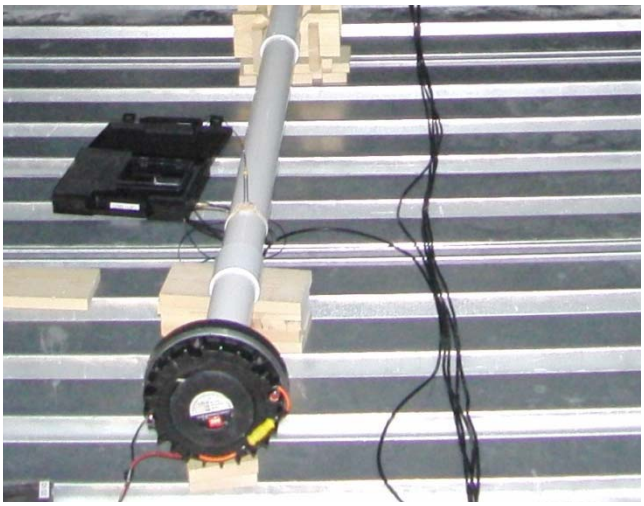

Figure 1. Picture of the plane wave tube. This tube is constructed out of 5.08 cm PVC pipe.

Some typical waveforms that we measured are shown in Figs. 2 and 3. The initially sinusoidal case is shown in Fig. 2, and the initially narrowband Gaussian noise case is shown in Fig. 3. For both cases, both the data at the first microphone (black) and the data for the farthest microphone (red) are shown. Nonlinear distortion is evident in both cases. In both cases, the initial sinusoidal or central frequency is 1500 Hz.

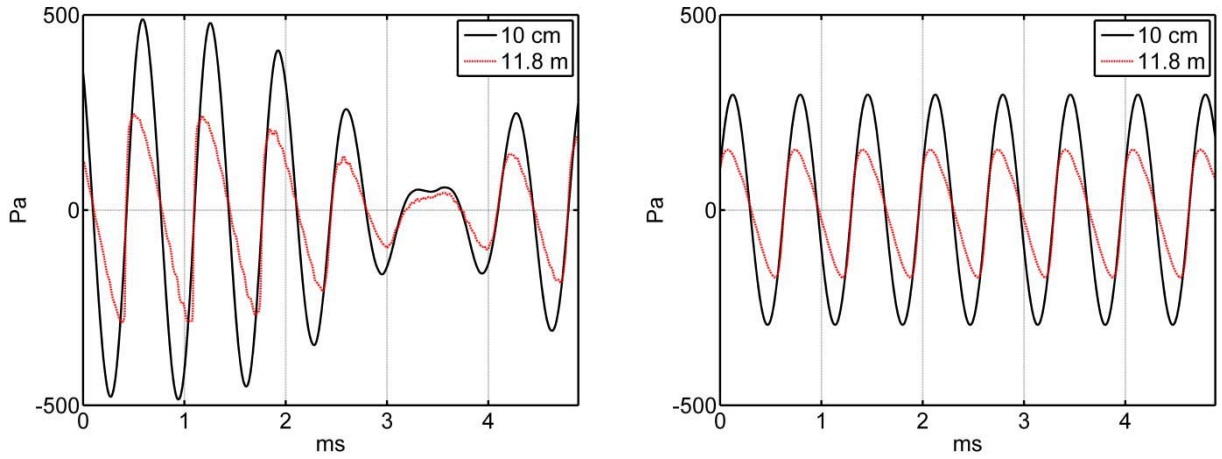

Figures 2 (left) and 3 (right). Typical sinusoidal (left) and narrowband noise (right) signal measurements. Nonlinear steepening is evident as the signal propagates through the plane wave tube.

Typical output spectra for the sinusoidal, narrowband, and broadband propagation are shown in Figs. 4 and 5. The initial amplitudes were chosen such that all of the signals would have approximately the same rms amplitude. The overall levels at the first microphone were about 140 dB re 20μPa. Figure 4 shows the spectrum at the first microphone and Fig. 5 shows the spectrum at the farthest microphone. Figure 4 exhibits the nonlinear distortion of the spectra. Notice the harmonic growth in the sinusoidal and narrowband cases, and the growth of the higher and lower frequencies in the narrowband and broadband cases. Because the low-frequency energy comes from difference frequencies, it makes sense that the single-frequency sinusoidal case does not exhibit such growth.

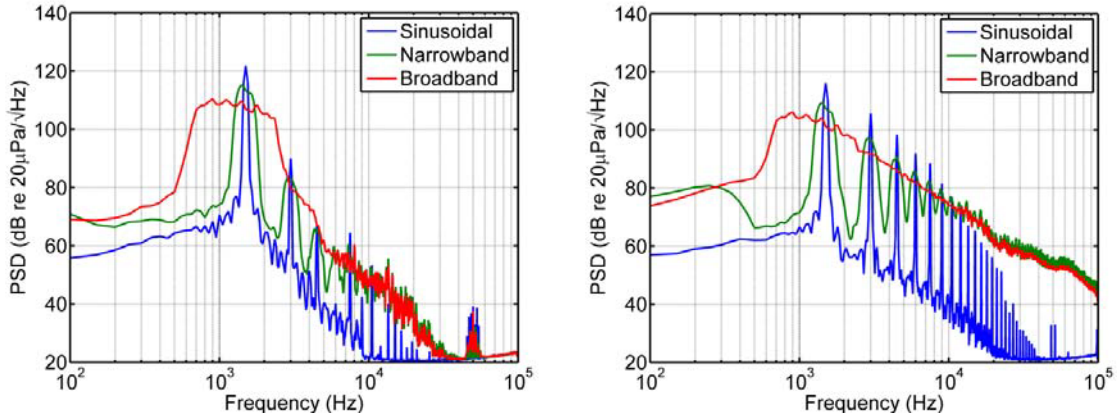

Figures 4 (left) and 5 (right). Typical spectra measurements near the source (left) and at 11.8 m from the source (right). Nonlinear harmonic generation is evident in the sinusoidal and narrowband cases.

III. DATA ANALYSIS

One way to study evolution of a signal is to look at how the statistics of the signal change over distance. We have chosen to analyze the estimated probability density functions (the PDFs calculated as outlined by Bendat and Piersol[8]) and the skewness (third standardized moment) of the pressure amplitudes and a first-order estimate of their time derivatives. For reference, the skewness of a random variable x is defined as

$$S_x = \frac{1}{N-1}\sum_{i=1}^{N}\frac{(x_i-\mu_x)^3}{\sigma_x^3} \tag{2}$$

where N is the number of samples, x_i is the i^{th} sample of x, μ_x is the mean of x, and σ_x is the standard deviation of x.

The validation of using PDF estimates and skewness is as follows: Shepherd, et al.[9] showed that for a lossless, planar signal, the estimated PDF of the pressure amplitudes starts in a bimodal distribution and does not change until after the shock formation distance, where the PDF estimate starts to evolve into a uniform distribution. Shepherd, et al. also showed that the pre-shock evolution of the PDF estimate of the first-order time derivative of the pressure, p_t, was quite dramatic, starting bimodal but becoming significantly positively skewed as a result of the nonlinear waveform steepening. Thus the skewness of p_t, S_{p_t}, may be considered for a figure of merit describing the evolution of a signal towards the shock formation distance.

To benchmark our figures, we first analyzed the statistics for an initially sinusoidal signal. Figure 6 shows an estimate of the PDF for the measured pressure amplitude of a sine wave. Notice the bimodal nature. There is a slight drift of the PDF estimate to emphasize negative pressures as the wave propagates, which is caused by dispersion in the pipe.[11,12] Figure 7 shows a PDF estimate of p_t. Initially it is also bimodal, as expected; however, as the signal propagates, it becomes heavily skewed toward large positive values as the waveform distorts. In Fig. 8 several values of S_{p_t} are plotted as a function of $x/\bar{x}_S$. In order to obtain greater resolution, multiple signals of different amplitudes with an approximate range of 128-148 dB re 20μPa were used to create this plot. (Similar means were used for the plots in Figs. 11-15.) Near the source, the skewness increases linearly from zero, but around the shock formation distance there is a strong positive bend in S_{p_t} before coming to some asymptotic value. We will use this characteristic shape to guide a statistics-based definition of a characteristic shock formation distance.

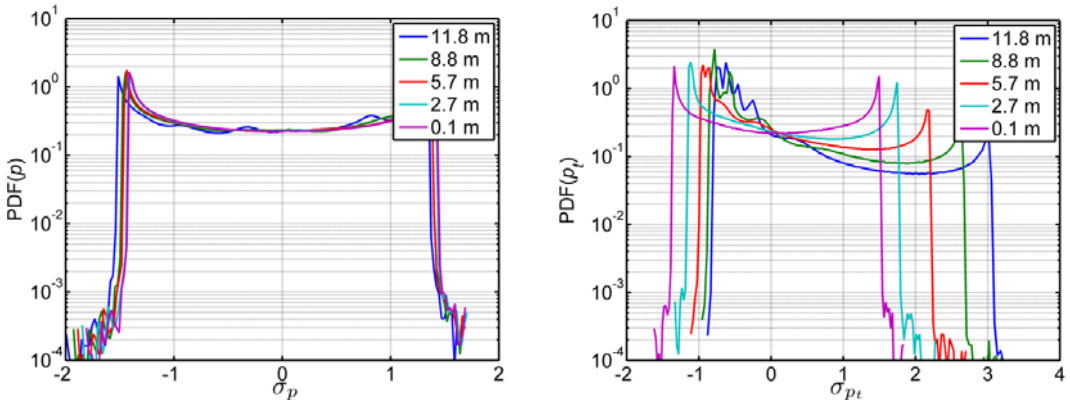

Figures 6 (left) and 7 (right). Estimates of probability density functions (PDF) of pressure amplitudes (left) and first-order time derivative of pressure (right) for an initially sinusoidal signal.

Note that $\bar{x}_S$ used here is the lossless shock formation distance. In practice, because of the boundary layer losses, the actual shock formation distance occurs beyond $x/\bar{x}_S = 1$; it is closer to 1.3.

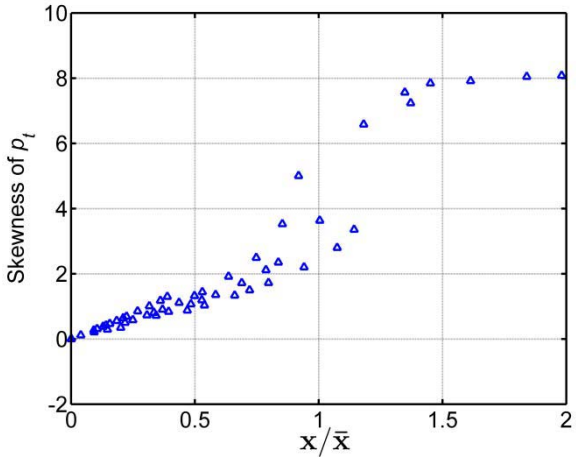

Figure 8. Values of skewness of the first-order time derivative of pressure amplitudes of an initially sinusoidal signal as a function of distance. The definition of $\bar{x}_s$ was used for $\bar{x}$.

Now we consider the propagation of Gaussian narrowband noise. The initial PDF, shown in Fig. 9, is quite Gaussian, as is the final PDF, shown in Fig. 10. Again, due to dispersion, the PDF drifts to the negative. The PDF of the first time derivative of the pressure amplitudes shows strong skewing to the positive from the steepening and shocking of the waveform. Again, the skewness, shown in Fig. 11, shows a strong bend. However, instead of being anywhere close to $\bar{x}_N$ as defined by Gurbatov and Rudenko, it shows up much earlier. It is noted that, in our experiments, the statistical evolution for broadband noise appears essentially the same as the narrowband noise in Figs. 9, 10, and 11. The central frequency was used as the characteristic frequency for these analyses: $\omega_c = \omega_0$, and so $\bar{x}_B = \bar{x}_N$.

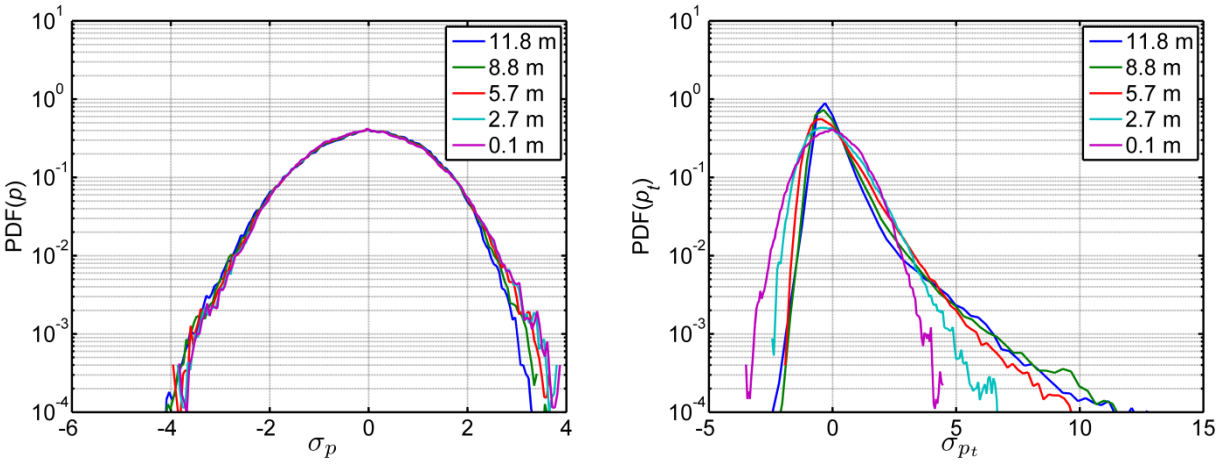

Figures 9 (left) and 10 (right). Estimates of probability density functions (PDF) of pressure amplitudes (left) and first-order time derivative of pressure (right) for initially Gaussian narrowband noise.

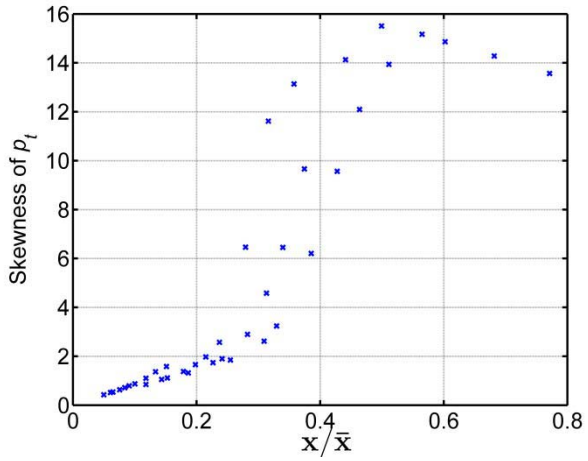

Figure 11. Values of skewness of the first-order time derivative of pressure amplitudes of initially Gaussian narrowband noise as a function of distance. The definition of $\bar{x}_N$ was used for $\bar{x}$.

It is desirable that the evolution of S_{p_t} would align for both initially sinusoidal signals and initially Gaussian noise when normalized by a proper characteristic shock formation distance. However, when these values are plotted on the same axis using $\bar{x}_N$ this does not happen (see Fig. 12). Notice that the noise and the sinusoidal values of S_{p_t} do have the same general characteristics (a linear increase from zero until a certain distance, where the skewness shoots up, followed by an asymptotic maximum value), but are on different scales. It is possible to correct this offset by inserting a correcting factor into $\bar{x}_N$.

In Fig. 13 the value for $\bar{x}_N$ has been modified by a factor of about 3.43. This value was found by taking the ratio of the slopes of the linear portions of the skewness plots (the slopes were found using a linear regression with the curve fitting tool in MATLAB). Notice that this factor aligns all major features of the data sets excepting the value of the asymptotic value of skewness. Because the noise pressure values measured in this experiment had a Gaussian distribution, they did not have definite upper bound to the amplitudes, while the initially sinusoidal signal did, even though they had the same rms pressure value. This would explain why the asymptotic value of S_{p_t} would be higher for noise.

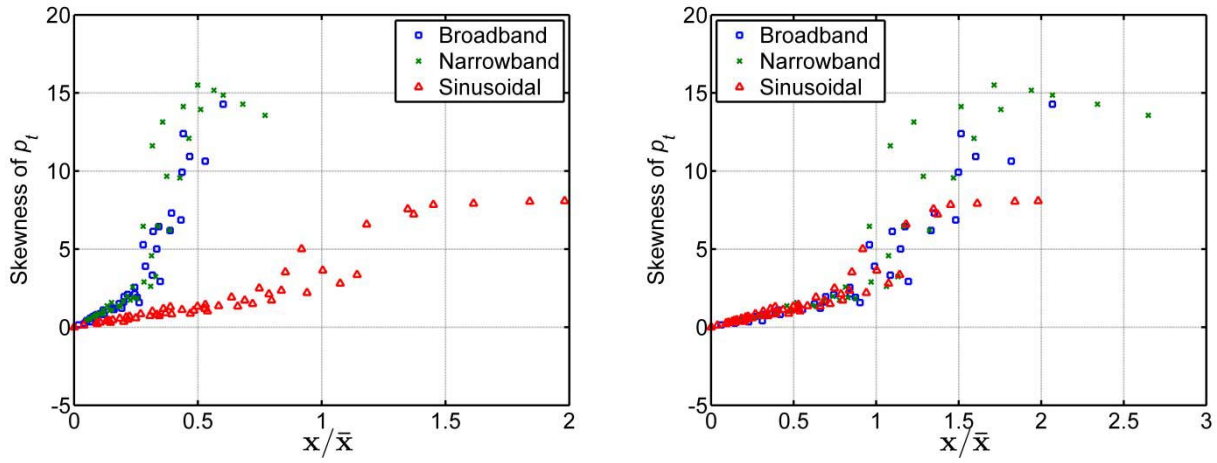

Figure 12 (left). Comparison of values of S_{p_t} for initially sinusoidal signals with initially Gaussian broadband and narrowband noise. The expression for $\bar{x}$ is $\bar{x}_S$ and $\bar{x}_N$ for the sinusoidal signals and noise signals respectively. Figure 13 (right). Same as Fig. 12, but with a corrective factor of about 3.43 applied to the distances for the noise signals.

To determine if this factor was unique to ω_c = 1500 Hz, we repeated the same tests for 1000 Hz and 2000 Hz. The plots in Figs. 14 and 15 have the same factor of about 3.43 was used to modify $\bar{x}_N$ in order to see if the evolutions align as they did in the ω_c = 1500 Hz case. The linear portions align and all major features are matched, again except the asymptotic skewness value. Thus, for the range of frequencies from 1000 Hz to 2000 Hz, the statistics-based scaling factor for defining a characteristic shock formation distance appears to be robust.

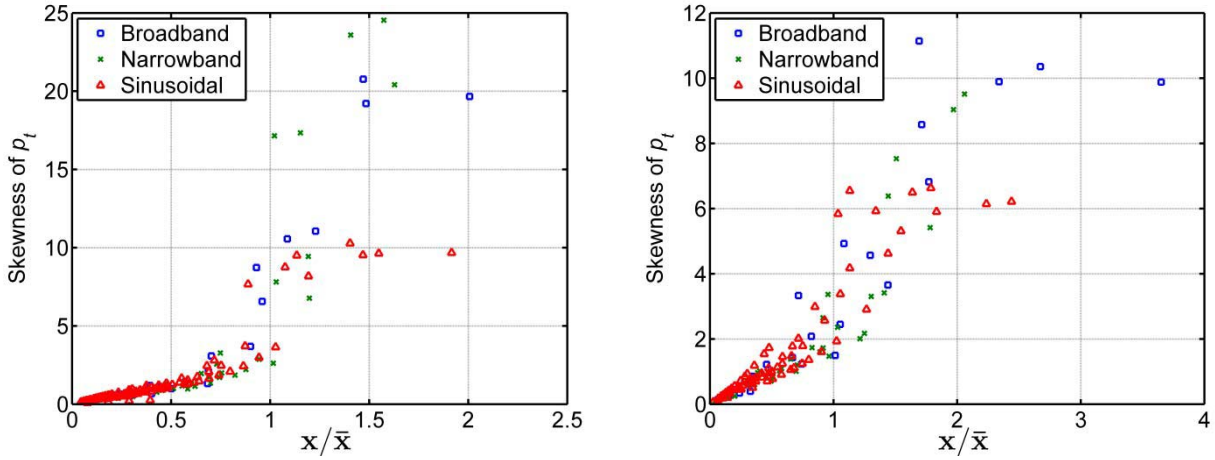

Figures 14 (above) and 15 (below). Similar plots as Fig. 13, but with different central frequencies: 1000 Hz (above) and 2000 Hz (below). The same factor of about 3.43 was used. Notice the agreement of the data as a function of distance.

IV. CONCLUSIONS

From the above analysis, it is seen, from a statistical standpoint, that $\bar{x}_N$ and $\bar{x}_B$ are not appropriate definitions for a characteristic shock formation distance for Gaussian noise of any bandwidth. A better definition, $\bar{x}_G$, can be obtained by adjusting $\bar{x}_N$ as follows:

$$\bar{x}_G = \frac{\rho_0 c_0^3}{\beta \omega_0 \Sigma_G}, \qquad \Sigma_G = \kappa_G \sigma_p, \tag{3}$$

where κ_G is approximately equal to 3.43 for Gaussian noise (but is currently limited to our tests with characteristic frequencies from 1000 Hz to 2000 Hz). It appears that κ_G is independent of bandwidth; this is the reason that the factor has been applied to the amplitude term.

The physical interpretation for Σ_G is found by analyzing the differences between $\bar{x}_S$ and $\bar{x}_N$ (see Table 1). In defining $\bar{x}_S$, it is not the rms pressure that dictates the shock formation distance, but rather the peak pressure excursions. Thus, Σ_G can be viewed as an effective peak pressure amplitude. It follows that the pressure amplitudes

greater than κ_G standard deviations are primarily responsible for the evolution of the skewness of the derivative and our definition of the shock formation distance. For an initially Gaussian waveform, this is the outermost 1.6% of the amplitudes (the tails of the distribution).

This interpretation of Σ_G also explains why $\bar{x}_G$ is independent of bandwidth. Because the distributions were Gaussian for each case, the only statistical variable is the standard deviation. Since Σ_G accounts for this, there is nothing that statistically differs $\bar{x}_G$ for narrowband noise from $\bar{x}_G$ for broadband noise. This assumes that the central frequency is a good characteristic frequency for broadband noise.

V. FUTURE WORK

We plan to continue developing the above analysis of the shock-developing region of the waveform evolution. To determine if the interpretation of the factor κ_G is correct, we plan to widen the frequency range used, change source spectral shapes and try other statistical distributions than Gaussian. Expanding the number of statistical distributions is particularly important because jet and rocket noise are not Gaussian.

We would also like to see how the value of $\bar{x}_G$ compare to values found using other analyses. Examples of these analyses are temporal, such as examining the characteristic number of shocks per zero crossing and percentage of waveform in a shock-like state, and spectral, such as examining the growth of harmonics and the spectral roll-off in the higher frequencies.

VI. ACKNOWLEDGEMENTS

We would like to acknowledgement Anthony Atchley and Micah Shepherd for useful conversations leading to the physical interpretation of κ_G.

VII. REFERENCES

1 D. T. Blackstock, "Nonlinear propagation of jet noise," Proceedings of the third Interagency Symposium on University Research in Transportation Noise, 389-397 (1975).

2 K. L. Gee, V. W. Sparrow, M. M. James, J. M. Downing, C. M. Hobbs, T. B. Gabrielson, and A. A. Atchley, "The role of nonlinear effects in the propagation of noise from high-power jet aircraft," J. Acoust. Soc. Am. **123** (6), 4082-4093 (2008).

3 S. A. McInerny and S. M. Olcmen, "High-intensity rocket noise: Nonlinear propagation, atmospheric absorption, and characterization," J. Acoust. Soc. Am. **117** (2), 578-591 (2005).

4 K. L. Gee, A. A. Atchley, T. B. Gabrielson, and V. W. Sparrow, "Preliminary Analysis of Nonlinearity in Military Jet Aircraft Noise Propagation," AIAA Journal **43** (6), 1398-1401 (2005).

5 R. J. Kenny, C. Hobbs, and K. Plotkin, "Measurement and Characterization of Space Shuttle Solid Rocket Motor Plume Acoustics", in *15th AIAA/CEAS Aeroacoustics Conference* (AIAA, Miami, Florida, 2009).

6 D. T. Blackstock, M. F. Hamilton, and A. D. Pierce, "Progressive Waves in Lossless and Lossy Fluids", in *Nonlinear Acoustics*, edited by M. F. H. and D. T. Blackstock (Academic Press, 1998), pp. 65-150.

7 S. N. Gurbatov and O. V. Rudenko, "Statistical Phenomena", in *Nonlinear Acoustics*, edited by M. F. Hamilton and D. T. Blackstock (Academic Press, 1998), pp. 377-398.

8 J. S. Bendat and A. G. Piersol, *Random Data*. (2010), Fourth ed.

9 M. R. Shepherd, K. L. Gee, and A. D. Hanford, "Evolution of statistical properties for a nonlinearly propagating sinusoid," J. Acoust. Soc. Am., in press (2011).

10 D. F. Pernet and R. C. Payne, "Non-linear propagation of signals in air," J. Sound Vib. 17 (3), 383-396 (1971).

11 F. M. Pestorius, PhD Thesis, The University of Texas at Austin, 1973.

12 M. F. Hamilton, Yu. A. Il'inskii, and E. A. Zabolotskaya, "Dispersion", in *Nonlinear Acoustics*, edited by M. F. Hamilton and D. T. Blackstock (1998), pp. 151-175.